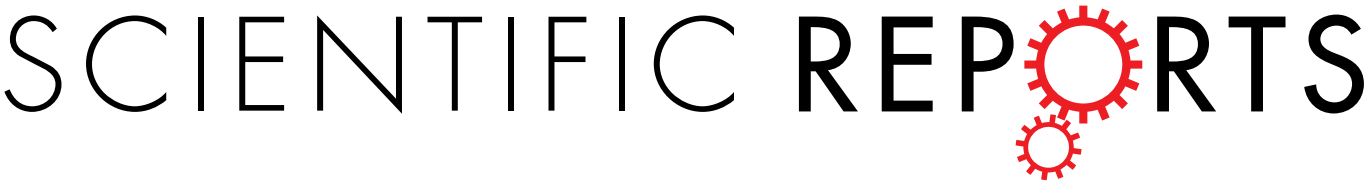

OPEN

Tunable electron heating induced giant magnetoresistance in the high mobility GaAs/AlGaAs 2D electron system

Received: 30 September 2016
Accepted: 10 November 2016
Published: 07 December 2016

Zhuo Wang[1], R. L. Samaraweera[1], C. Reichl[2], W. Wegscheider[2] & R. G. Mani[1]

Electron-heating induced by a tunable, supplementary dc-current (I_{dc}) helps to vary the observed magnetoresistance in the high mobility GaAs/AlGaAs 2D electron system. The magnetoresistance at $B = 0.3$T is shown to progressively change from positive to negative with increasing I_{dc}, yielding negative giant-magnetoresistance at the lowest temperature and highest I_{dc}. A two-term Drude model successfully fits the data at all I_{dc} and T. The results indicate that carrier heating modifies a conductivity correction σ_1, which undergoes sign reversal from positive to negative with increasing I_{dc}, and this is responsible for the observed crossover from positive- to negative- magnetoresistance, respectively, at the highest B.

Giant magnetoresistance (GMR) denotes a large change in the electrical resistance under the application of a magnetic field and the GMR effect observed in magnetic metallic multilayers (MMM) has now become the canonical GMR effect since it transformed the magnetic hard disk storage and memory industries[1–6]. Physically, the MMM-GMR arises as an applied magnetic field re-aligns the magnetic moments of the successive ferromagnetic layers, which are separated by the nonmagnetic layers[1,2,5,6]. Although not as well known, GMR also occurs in both magnetic and non-magnetic semiconductor systems[3]. Semiconductor GMR is particularly interesting for applications because of the expected ease of integration of associated devices with typical semiconductor electronics[3]. As a consequence, the study of potential new mechanisms for realizing GMR in semiconductors has been a useful line of basic research[7–10]. Semiconductor GMR in disordered 2D electronic systems has also been a topic of interest from the fundamental physics perspective[11–28], providing insight into weak localization[11,17], weak anti-localization[11,17], electron-electron interaction-induced magnetoresistance[11,14–16,18,19,22,23], metal-insulator transitions induced by a magnetic field[29], and GMR in the quantum Hall regime[30,31].

Here, we study and model an interesting new mechanism for inducing- and controlling- GMR in a two-dimensional semiconductor system. While previous studies have examined electric field control of magnetoresistance[7,9,10], we show that a supplementary dc-current-bias and associated carrier heating in an ac- and dc- current biased high mobility 2DES provides for a current dependent "non-ohmic" decrease in the conductivity with increasing dc current bias in the absence of a magnetic field, and this effect leads to a *dc-current tunable GMR* in the presence of 100's-of-millitesla-type magnetic fields. Thus, the effect identifies a simple new method for setting the magnitude of the GMR effect as desired, in a semiconductor system.

The ultra high mobility GaAs/AlGaAs system has been the subject of intense magnetotransport studies at high filling factors or low magnetic fields because improvements in material quality in this 2D electron system have led to a steady stream of spectacular new phenomena such as the microwave radiation-induced zero-resistance states and associated magnetoresistance oscillations[32–72], magnetoresistance that depends on the electron-electron interactions[14–16,18,23], device size[19,21,26], scatterer type[20,22,24,27], temperature, carrier density[24], and orientation of magnetic field[25], giant resonances at the second harmonic of cyclotron resonance[73–75], etc. The negative magnetoresistance observed in the GaAs/AlGaAs system was initially viewed as a manifestation of disorder-induced electron-electron interaction effect[14–16]. However, features such as the concurrent absence of a Hall-effect correction[26], dependence upon scattering type[27], etc., have led to new experimental and theoretical interest. Following

[1]Department of Physics and Astronomy, Georgia State University, Atlanta, GA 30303, USA. [2]Laboratorium für Festkörperphysik, ETH-Zürich, Zürich 8093, Switzerland. Correspondence and requests for materials should be addressed to R.G.M. (email: mani.rg@gmail.com)

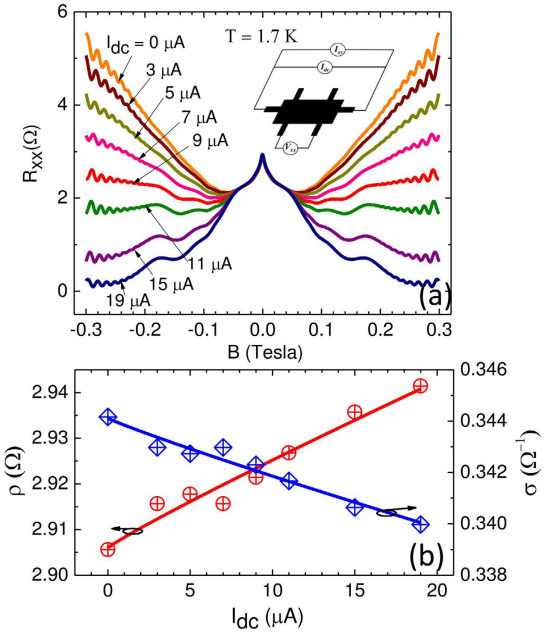

Figure 1. Tunable giant magnetoresistance induced by a dc current bias in a GaAs/AlGaAs heterostructure 2DES. (**a**) Magnetoresistance, R_{xx}, vs. the magnetic field, B, at different dc currents. The inset shows a schematic of the measurement. (**b**) The resistivity (red) and conductivity (blue) vs. I_{dc} in the absence of magnetic field.

upon this interest, we report on an effect which is unexpected within the context of previous theory - a current tunable, carrier-heating-induced negative GMR in the GaAs/AlGaAs 2D system.

Results

Figure 1(a) shows the magnetoresistance at $T = 1.7$ K, as I_{dc} is varied from 0 to 19 μA. The figure shows that R_{xx} below $B = 0.05$ T is hardly influenced by the I_{dc}. We found that this part could be simply represented by $\Delta R_{xx} = A\ln(B_0/B)$[26]. On the other hand, above $B = 0.05$ T, the R_{xx} vs B traces change substantially with the applied I_{dc}. In particular, the observed positive magnetoresistance above $B = 0.05$ T at $I_{dc} = 0\,\mu A$ progressively decreases with increasing I_{dc} and results in $\geq$90% negative GMR at $I_{dc} = 19\,\mu A$ and B = 0.3 T. Above $B = 0.05$ T, the magnetoresistance traces also exhibit, to $B \approx 0.2$ T, magnetophonon oscillations[76] which increase in amplitude with increasing I_{dc}. This feature, to be examined elsewhere, is one signature of I_{dc}-induced heating. Finally, at the highest B, $B \geq 0.2$ T, Fig. 1(a) shows Shubnikov de Haas (SdH) oscillations, which appear to be reduced in amplitude with increasing I_{dc} - yet another signature of I_{dc} induced electron heating.

In order to convey the variation of the resistivity (ρ) and conductivity (σ) under the influence of I_{dc}, Fig. 1(b) exhibits the ρ (in red) and σ (in blue) vs. I_{dc} at $B = 0$ T. Without heating, one expects ρ and σ to remain constant under changing I_{dc}, as a consequence of "Ohm's Law". The figures show, however, that σ is reduced with increasing I_{dc}, roughly by 1.3% for $\Delta I_{dc} = 19\,\mu A$. Thus, the total current-dependent conductivity in the absence of a magnetic field can be written as $\sigma(I) = \sigma_0 + \sigma_1'(I_{dc})$, where $\sigma(I)$ is the current dependent conductivity. Here, the effect of the ac-current is not included since it is relatively small in magnitude.

To fit the B-dependent GMR results of Fig. 1(a), following previous work[26], $\sigma \rightarrow \sigma_{xx}$, resulting in $\sigma_{xx} = \sigma_{xx}^0 + \sigma_{xx}^1(I) = \sigma_0/[1 + (\mu_0 B)^2] + \sigma_1/[1 + (\mu_1 B)^2]$. [Similarly, $\sigma_{xy} = \sigma_{xy}^0 + \sigma_{xy}^1(I) = \sigma_0\mu_0 B/[1 + (\mu_0 B)^2] + \sigma_1\mu_1 B/[1 + (\mu_1 B)^2]$]. Here, μ_1 is a parametric mobility in the Drude model[26]. Since $L/W = 1$, we set the diagonal resistance $R_{xx} = \rho_{xx}$, the diagonal resistivity, and $\rho_{xx} = \sigma_{xx}/[{\sigma_{xx}}^2 + {\sigma_{xy}}^2]$ (similarly, the off-diagonal resistivity is $\rho_{xy} = \sigma_{xy}/[{\sigma_{xx}}^2 + {\sigma_{xy}}^2]$). Here, $\sigma_0 = n_0\mu_0 e$, where n_0 and μ_0 are the electron density and mobility in the 2D electron system. To account for the I_{dc} independent magnetoresistance for $B \leq 0.05$ T, the afore-mentioned additional $\ln(B_0/B)$ term was included. Hence, the magnetoresistance data trace was fit to $R_{xx} = A\ln(B_0/B) + \sigma_{xx}/(\sigma_{xx}^2 + \sigma_{xy}^2)$. Here, A and B_0 were pre-determined by fitting the $B \leq 0.05$ T data, n_0 is held constant versus I_{dc} and T, while μ_0 is held constant versus I_{dc} but allowed to vary with T. Note that σ_1 and μ_1 are the fundamental parameters that serve to characterize the giant magnetoresistance (GMR) and its change with I_{dc}. Although there are four parameters, n_0, μ_0, σ_1 and μ_1 here, at a given T, only σ_1 and μ_1 were allowed to vary with I_{dc}. The fits to the 1.7 K data of Fig. 1(a) are presented in Fig. 2(a), and the fit parameters are summarized in Table (1). Figure 2(a) indicates a good description of the non-oscillatory portion of the data by this empirical fit.

The variation of the fit-obtained parameters σ_1 and μ_1, vs. I_{dc}, are shown in Fig. 2(b) and (c), respectively. Figure 2(b) shows that σ_1 is initially positive, then it gradually decreases, and turns negative above around $I_{dc} = 11\,\mu$A while continuing the trend at higher I_{dc}. Thus, $d\sigma_1/dI_{dc} \leq 0$ recalls the observed $d\sigma/dI_{dc} \leq 0$ in Fig. 1(b). The observed variation in the σ_1 vs. I_{dc} correlates with the progressive I_{dc} induced change in R_{xx} from overall positive- to overall negative GMR to $B = 0.3$ T. Note also that $I_{dc} \geq 11\,\mu$A allows for negative conductivity in σ_1,

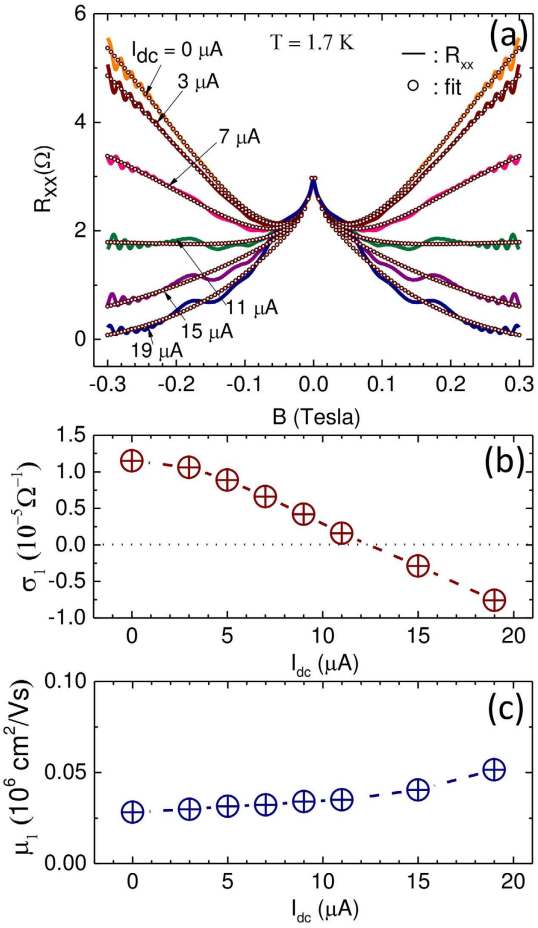

Figure 2. Model fits of the magnetoresistance in a GaAs/AlGaAs 2D electron device. (**a**) Multi-conduction model fits of giant magnetoresistance for various I_{dc}. Solid lines represent data, and symbols represent fit. (**b**) Fit parameter σ_1 vs. I_{dc}. Dashed line is a guide to the eyes. (**c**) Model parametric mobility, μ_1, vs. I_{dc}.

$n_0(10^{11}cm^{-2})$	$\mu_0(10^6cm^2/Vs)$	$I_{dc}(\mu A)$	$\sigma_1(10^{-5}\Omega^{-1})$	$\mu_1(10^6cm^2/Vs)$
2.4	11.56	0	1.15	0.0282
2.4	11.56	3	1.06	0.0298
2.4	11.56	7	0.66	0.0322
2.4	11.56	11	0.16	0.0351
2.4	11.56	15	−0.29	0.0404
2.4	11.56	19	−0.76	0.0515

Table 1. Fit parameters extracted from empirical data fit at 1.7 K. Here, n_0 and μ_0 are the two-dimensional electron density and mobility, respectively. σ_1 represents the conductivity correction which describes the magnetoresistance and μ_1 represents the associated parametric mobility.

i.e., $\sigma_1 \leq 0$. Since the parameters in Table 1 suggest that $|\sigma_1| << |\sigma_0|$, the negative σ_1 is manifested as a resistance correction at $B = 0$ T and a B-dependent (negative) magnetoresistance[26]. Figure 2(c) conveys that the fit parameter μ_1 increases gently with I_{dc}.

Similar measurements of R_{xx} vs. B were carried out at higher temperatures. Figure 3 shows I_{dc} parametrized R_{xx} vs B data-traces at $T = 1.7$ K, 2.7 K, 3.4 K, and 4.2 K, with each data set sequentially offset by 2 Ω. At each T, overall positive magnetoresistance is observable at the highest B for $I_{dc} = 0\,\mu A$. However, as I_{dc} is increased, the positive magnetoresistance is progressively reduced and transformed into negative magnetoresistance at the highest I_{dc} (the characteristic T for this crossover depends on whether or not one includes the weak-localization-like term in the vicinity of $B = 0$ in the consideration). Further, at $T = 4.2$ K, magnetophonon oscillations are apparent at $I_{dc} = 0\,\mu A$ and they are progressive reduced in amplitude with increasing I_{dc}. On the other hand, at $T = 1.7$ K, magnetophonon oscillations are not readily apparent at $I_{dc} = 0\,\mu A$ and become more apparent with increasing I_{dc}. Both these features can be understood as a consequence of the well-known non-monotonic variation of the magnetophonon oscillation amplitude with T[76]. That is, while the magnetophonon oscillations vanish in the "low-T"

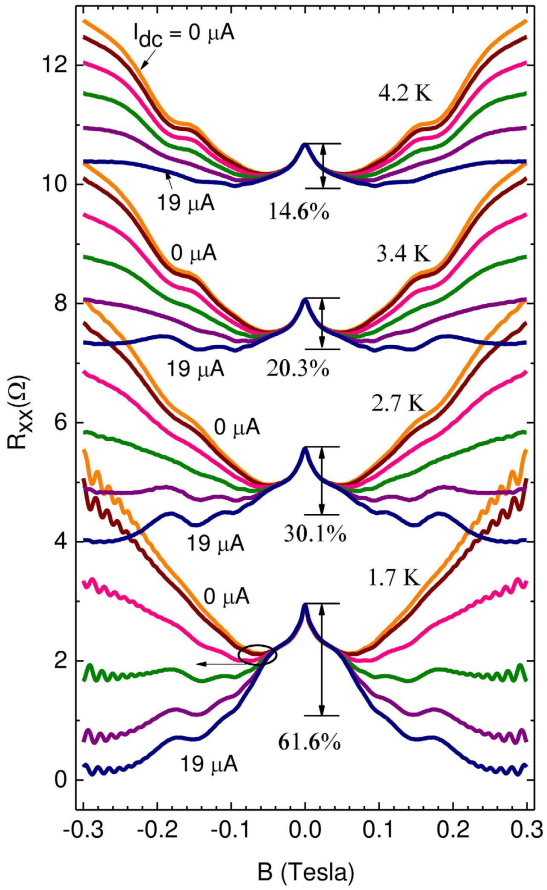

Figure 3. Temperature dependence of the magnetoresistance and its dependence on I_{dc}. This panel shows the R_{xx} vs. B, at various bath temperatures, with the $I_{dc} = 0$, 3, 7, 11, 15 and 19 μA as the parameter. Here, the data sets at different T have been sequentially offset by 2Ω, for the sake of presentation. In addition, the percentage change in the magnetoresistance to B = 0.1 Tesla, at the highest current, is indicated for each temperature.

limit, they increase in the amplitude with increasing temperature up to some characteristic temperature, while further temperature increase then leads to a reduction in the oscillation amplitude. Since the 4.2 K traces suggests strong amplitude at $I_{dc} = 0\ \mu A$, and the increase of I_{dc} leads to a reduction in the oscillation amplitude, it is apparent that this data set represents the "optimally heated" to the "over-heated" regime, where the magnetophonon oscillation amplitude decreases with a further increase in the temperature, due to the dc-current induced heating. On the other hand, Fig. 3 shows that at 1.7 K, the magnetophonon oscillations are barely perceptible at 1.7 K and they become stronger with increasing I_{dc}. Thus, this data set represents the "under-heated" to "optimally heated" regime, where increasing the temperature with the I_{dc} increases the oscillation amplitude. Thus, the observed trends in the amplitude of the magnetophonon oscillations also confirm that the I_{dc} serves to heat the system, as reasoned earlier.

The non-oscillatory part of the T-dependent data sets of Fig. 3 were also fit with the multiconduction model; the results are shown in Fig. 4(a) while the fit parameters are summarized in Table 2. Here, symbols represent the fit while the lines represent data. As indicated by Fig. 4, the empirical model succeeds in describing the data at all temperatures and I_{dc}. The extracted fit parameter σ_1 is shown in Fig. 4(b) as a function of I_{dc}. Similar to its behavior at $T = 1.7$ K, the fit extracted σ_1 decreases with increasing I_{dc} at all T. However, the magnitude of the decrease in σ_1 with increasing I_{dc} is more pronounced at lower T. Further, the crossover from positive to negative GMR at $B = 0.3\ T$ is only observed $T = 1.7$ K and $T = 2.7$ K, while at higher T, there is only mostly positive GMR. This feature can be correlated with the point that negative magnetoresistance is only observable when $\sigma_1 < 0$. As mentioned, the fit extracted μ_1 was only allowed to vary with I_{dc} but not with T. As a consequence, the fit extracted μ_1 vs. I_{dc} traces at all T, not shown, were identical to the Fig. 2(c). Figure 4(c) exhibits the T-dependence of σ_1 at various I_{dc}. At small I_{dc}, σ_1 is essentially independent of T. On the other hand, at $I_{dc} = 19\ \mu A$, σ_1 decreases strongly with decreasing temperature, and the crossover from positive- to negative- σ_1 occurs around $T = 3$ K. Thus, at $I_{dc} = 19\ \mu A$, negative magnetoresistance due to heating becomes observable below $T = 3.0$ K.

Discussion

The experimental results shown here in Fig. 1(b) indicate that steady state specimen heating induced by the application of a supplementary I_{dc} gives rise to a "non-ohmic" current-dependent conductivity with $d\sigma/dI_{dc} \leq 0$. Under the same steady state I_{dc}-induced non-equilibrium conditions, the specimen exhibits a I_{dc} dependent

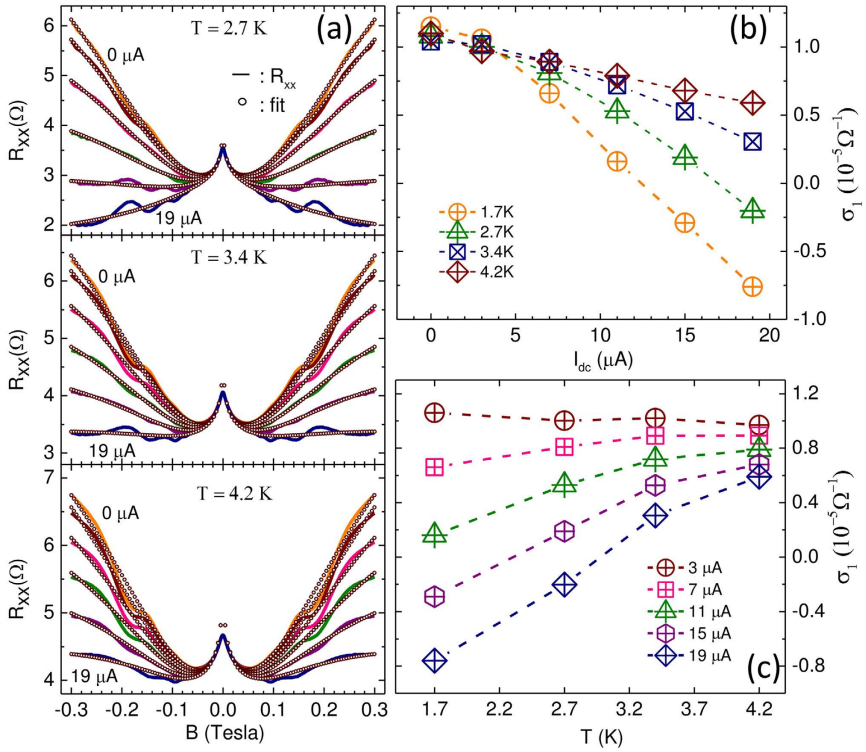

Figure 4. Data fits of the magnetoresistance at different I_{dc} and temperatures. (**a**) The I_{dc}-dependent magnetoresistance is shown for various T with $I_{dc} = 0$, 3, 7, 11, 15 and 19 μA, along with the empirical data fits. Here, solid lines represent data and symbols represent fits. (**b**) This plot shows σ_1, which is extracted from data fits, vs. I_{dc}, at different temperatures. (**c**) This plot shows σ_1 vs. T, at different I_{dc}.

T(K)	$n_0(10^{11}cm^{-2})$	$\mu_0(10^6cm^2/Vs)$	$I_{dc}(\mu A)$	$\sigma_1(10^{-5}\Omega^{-1})$	$\mu_1(10^6cm^2/Vs)$
1.7	2.4	11.56	0	1.15	0.0282
			19	−0.76	0.0515
2.7	2.4	9.16	0	1.08	0.0282
			19	−0.20	0.0515
3.4	2.4	7.60	0	1.04	0.0282
			19	0.31	0.0515
4.2	2.4	6.77	0	1.10	0.0282
			19	0.059	0.0515

Table 2. Summary of the temperature dependence of the fit parameters extracted from the data fits. Here, n_0 and μ_0 are the two-dimensional electron density and mobility, respectively. σ_1 represents the conductivity correction which describes the magnetoresistance and μ_1 represents the associated parametric mobility.

magnetoresistance to $B = 0.3$ T, which can be successfully described by a two-term Drude model including a second conduction term with the parameters σ_1 and μ_1. Data fitting helps to extract these parameters and shows that $d\sigma_1/dI_{dc} \leq 0$, similar to $d\sigma/dI_{dc} \leq 0$. While $d\sigma/dI_{dc} \approx 10^2\Omega^{-1}/A$, the fit parameters show that $d\sigma_1/dI_{dc} \approx 1\Omega^{-1}/A$. This point suggests that all the conductivity change induced by the dc-current in Fig. 1(b) does not contribute towards the modification of the magnetoresistance described by σ_1 in Fig. 2(b). Thus, it appears that the dc-current modifies σ via several modes and not all these modes influence the magnetoresistance. Further, Fig. 4(b) shows that $d\sigma_1/dI_{dc}$ varies strongly with T. This feature suggests a role for the inelastic scattering length in influencing the GMR, as suggested previously[19], and its dependence on the I_{dc} and T. The previous fit-study indicated that a negative conductivity term with associated parametric mobility in a multiconduction model is sufficient to realize negative GMR in this 2D electron system[26]. This study shows that the application of I_{dc} helps to realize such a conductivity correction as a by-product of heating, leading to the observed negative GMR.

Previous theoretical and experimental studies on the effect of steady state heating on the energy distribution of electrons offer insights for our study. For example, experimental photoluminescense studies at a low lattice temperature (e.g., $T_L = 10$ K) have shown that the photoluminescence lineshape at the fixed lattice temperature broadens and red-shifts with the steady state heating due to terahertz radiation, while lineshape fits utilized to extract an effective (electron) temperature indicate the electron temperature, T_e, exceeds the lattice temperature, T_L, and the

difference $T_e - T_L$ becomes larger with increased terahertz photoexcitation[77]. Remarkably, concurrent studies of the electrical conductivity under the same steady state terahertz drive showed a *monotonic decrease* in the conductivity with increased terahertz photoexcitation which could also be described in terms of an effective (electron) temperature that exceeds T_L. Indeed, the T_e determined through the two different experiments showed good agreement. Thus, the energy distribution of electrons under steady state terahertz excitation induced heating could be characterized by an electron temperature that is elevated with respect to the lattice temperature, i.e., $T_e > T_L$[77]. Theoretical studies based on a steady state Boltzmann equation solution of the momentum and energy-balance equations taking into account the electron-LO phonon[78] and electron-deformation potential acoustic phonon interaction[79] confirmed that in such steady state drive experiments (i) the electron energy distribution can be characterized by an effective- and elevated- T_e, (ii) the electron-phonon interaction dominates both momentum and energy relaxation, (iii) hot electrons relax by emitting or absorbing phonons, which changes phonon number and leads to a phonon number that depends on the electron temperature, and (iv) phonon-drift is negligible[78,79].

Another detailed study of the energy loss mechanism in a low temperature 2DES including ballistic hot electron injection suggested that injecting mono-energetic hot electrons into a 2DES thermalizes the 2D electronic system to a temperature T_e that exceeds T_L when electron-electron scattering rate is large compared to inelastic scattering rate[80]. For hot electron injection energies below the LO phonon energy $E_{LO} = 36$meV, all the injected power is transferred via electron-electron scattering to a thermalized 2DES at an elevated T_e, and the associated energy is subsequently lost by energy balance to acoustic phonons. In such a situation, T_e is a proportional measure of the injected power, or vice-versa. For hot electron injection energies above the LO phonon energy, injected hot electrons could emit LO phonons before interacting with the 2DES, depending upon the LO phonon emission time, τ_{LO}, and the energy transferred to the 2DES per hot electron could then become the difference between the hot electron energy and the LO phonon energy[80].

In our experiment, the steady state heating is realized by injecting the supplementary dc current, not by terahertz photoexcitation or by mono-energetic hot electron injection. Yet, the above mentioned results imply that, since we are using the same GaAs/AlGaAs material system in the same low temperature limit, the electron-electron scattering rate likely exceeds the inelastic scattering rate, leading to I_{dc} heated electron system characterized by a $T_e > T_L$. Further, since the applied supplementary dc currents are modest, $I_{dc} \leq 19\,\mu$A, the effective energies associated with the injected electrons in the supplemental dc current are likely small compared to $E_{LO} = 36$ meV. (For $I_{dc} = 19\,\mu$A, and an upper bound resistance estimate based the Hall resistance $R_{xy} \approx 1\,k\Omega$ at $B = 0.3\,T$, it turns out that $eIR_{xy} = 19\,meV$, which is less than the $E_{LO} = 36$ meV). As a consequence, energy loss is expected to be through acoustic phonons. In this regime, the T_e should increase monotonically with increased I_{dc}. Since electron heating has been shown the reduce the electrical conductivity[77], and we observe and report a reduction in the conductivity with the increase of the supplementary I_{dc}, while correlating this observation with the characteristic heating-like reduction in the Shubnikov-de Haas oscillation amplitude with increased I_{dc} (Fig. 1), and the characteristic I_{dc} induced changes in amplitude of the magnetophonon oscillations (Figs 1 and 3), it is clear that the observed $d\sigma/dI_{dc} < 0$ (Fig. 1(b)) is a manifestation of electron heating induced correction to the conductivity, where the I_{dc} parametrically represents the electron temperature.

When the heating by I_{dc} produces a "non-ohmic" correction to the conductivity σ (Fig. 1(b)), the correction affects the second term in the two-term Drude model modifying, as shown by the modeling presented here, the character of the magnetoresistance. Simply put, the supplementary I_{dc} heats the electron system, producing a "non-ohmic" decrease in the conductivity. The decrease in the conductivity has the effect of progressively converting the positive magnetoresistance to the negative giant magnetoresistance because the non-ohmic term strongly influences the second term in the Drude model. The magnetoresistance then becomes manifest through the mathematical character of the model.

The practical interest in these results rests upon the possibility of tuning the magnetoresistance in the 2D electron system simply with the application of a supplementary I_{dc}. This suggests the possibility of GMR devices, without a gate-electrode, where the response may be set as desired after manufacture by adjusting dc-current bias with external circuitry. While it is not yet clear which physical channel influenced by the dc-current heating affects the magnetoresistance, these results show that such a channel exists in the 2D electron system. Identification of this channel and the optimization of the physical platform, which are topics for future study, are likely to result in improved control of the giant-magnetoresistance in the 2D electron system.

Methods

The high-mobility GaAs/AlGaAs heterostructures used in this study were grown by molecular-beam epitaxy (MBE), and patterned into Hall bar devices by photolithography. The 200 μm wide Hall bars included voltage probes spaced by $200\mu m$, which set the effective Length-to-Width (L/W) ratio $L/W = 1$. Electrical measurements were carried out using standard low frequency lock-in techniques. The electron mobility at temperature $T = 1.7$ K was $\mu \approx 10^7\, cm^2/Vs$ and the density was $n = 2.4 \times 10^{11}\, cm^{-2}$. The ac- and dc- currents were applied as shown in the inset of Fig. 1. The lock-in sourced ac current source was held constant at 2 μA, as a dc current was varied as desired under computer control. Typically, at a fixed T, magnetic field (B) sweeps of the lock-in detected diagonal voltage V_{xx} were collected at a series of constant I_{dc}. The data traces plotted in the Figs 1a, 2a, 3 and 4a report the magnetoresistance $V_{xx}^{ac}/I_{ac} = R_{xx}$. The sample was immersed in pumped liquid helium for these measurements over the range $1.7\,\text{K} \leq T \leq 4.2\,\text{K}$.

References

1. Baibich, M. N. *et al.* Giant magnetoresistance of (001) Fe/(001) CR magnetic superlattices. *Phys. Rev. Lett.* **61,** 2472–2475 (1988).
2. Tsang, C. H. *et al.* Design, fabrication, and performance of spin-valve read heads for magnetic recording applications. *IBM J. Res. Develop.* **42,** 103–116 (1998).
3. Heremans, J. Solid state magnetic field sensors and applications. *J. Phys. D: Appl. Phys.* **26,** 1149–1168 (1993).
4. Moser, A. *et al.* Magnetic recording: advancing into the future. *J. Phys. D: Appl. Phys.* **35,** R157 (2002).

5. Chappert, C., Fert, A. & Dau, F. N. V. The emergence of spin electronics in data storage. *Nat. Matl.* **6,** 813–823 (2007).
6. Ikeda, S. *et al.* Magnetic tunnel junctions for spintronic memories and beyond. *IEEE Trans. Elect. Dev.* **54,** 991–1002 (2007).
7. Wang, Y. *et al.* Electric-tunable magnetoresistance effect in a two-dimensional electron gas modulated by hybrid magnetic-electric barrier nanostructure. *Phys. Lett. A* **373** 1983–1987 (2009).
8. Yue, Z. *et al.* Large networks of vertical multi-layer graphenes with morphology- tunable magnetoresistance. *Nanoscale* **5,** 9283–9288 (2013).
9. Li, S. *et al.* Large, tunable magnetoresistance in nonmagnetic III-V nanowires. *NanoLett*. **15,** 8026–8031 (2015).
10. Modepalli, V. *et al.* Gate-tunable spin exchange interactions and inversion of magnetoresistance in single ferromagnetic ZnO nanowires. *ACSNano* **10,** 4618–4626 (2016).
11. Lee, P. A. & Ramakrishnan, T. V. Disordered electronic systems. *Rev. Mod. Phys.* **57,** 287–337 (1985).
12. Abrahams, E., Anderson, P. W., Licciardello, D. C. & Ramakrishnan, T. V. Scaling theory of localization: Absence of quantum diffusion in two dimensions. *Phys. Rev. Lett.* **42,** 673–676 (1979).
13. Fukuyama, H. Hall effect in two-dimensional disordered systems. *J. Phys. Soc. Jpn.* **49,** 644–648 (1980).
14. Paalanen, M. A., Tsui, D. C. & Hwang, J. C. M. Parabolic magnetoresistance from the interaction effect in a two-dimensional electron gas. *Phys. Rev. Lett.* **51,** 2226–2229 (1982).
15. Girvin, S. M., Jonson, M. & Lee, P. A. Interaction effects in disordered Landau-level systems in two dimensions. *Phys. Rev. B.* **26,** 1651–1659 (1982).
16. Houghton, A., Senna, J. R. & Ying, S. C. Magnetoresistance and Hall effect of a disordered interacting two-dimensional electron system. *Phys. Rev. B* **25,** 2196–2210 (1982).
17. Bergmann, G. Weak localization in thin films - a time-of-flight experiment with conduction electrons. *Phys. Repts.* **107,** 1–58 (1984).
18. Choi, K. K., Tsui, D. C. & Palmateer, S. C. Electron-electron interaction in GaAs-AlGaAs heterostructures. *Phys. Rev. B* **33,** 8216–8227 (1986).
19. Mani, R. G., von Klitzing, K. & Ploog, K. Magnetoresistance over the intermediate localization regime in GaAs/AlGaAs quantum wires. *Phys. Rev. B* **48,** 4571–4574 (1993).
20. Mirlin, A. D., Polyakov, D. G., Evers, F. & Wolfle, P. Quasiclassical negative magnetoresistance of a 2D electron gas: Interplay of strong scatterers and smooth disorder. *Phys. Rev. Lett.* **87,** 126805 (2001).
21. Mani, R. G. *et al.* Magnetoresistive response of a high mobility 2DES under electromagnetic wave excitation. *Physics of Semiconductors 2002 - Proceedings of the 26th International Conference Edinburgh, 29 July-2 August 2002*, IOP Conf. Series 171, eds.A. R. Long & J. H. Davies (IOP, Bristol, 2003) H112 (arXiv:cond-mat/0305507).
22. Gornyi, I. V. & Mirlin, A. D. Interaction-induced magnetoresistance: From the diffusive to the ballistic regime. *Phys. Rev. Lett.* **90,** 076801 (2003).
23. Li, L., Proskuryakov, Y. Y., Savchenko, A. K., Linfield, E. H. & Ritchie, D. A. Magnetoresistance of a 2D electron gas caused by electron interactions in the transition from the diffusive to the ballistic regime. *Phys. Rev. Lett.* **90,** 076802 (2003).
24. Bockhorn, L., Barthold, P., Schuh, D., Wegscheider, W. & Haug, R. J. Magnetoresistance in a high mobility two-dimensional electron gas. *Phys. Rev. B* **83,** 113301 (2011).
25. Hatke, A. T., Zudov, M. A., Reno, J. L., Pfeiffer, L. N. & West, K. W. Giant negative magnetoresistance in high mobility 2D electron systems. *Phys. Rev. B* **85,** 081304 (2012).
26. Mani, R. G., Kriisa, A. & Wegscheider, W. Size-dependent giant-magnetoresistance in millimeter scale GaAs/AlGaAs 2D electron devices. *Sci. Rep.* **3,** 2747; 10.1038/srep02747 (2013).
27. Bockhorn, L. *et al.* Magnetoresistance induced by rare strong scatterers in a high-mobility two-dimensional electron gas. *Phys. Rev. B* **90,** 165434 (2014).
28. Inarrea, J. Theoretical model for negative giant magnetoresistance in ultra high mobility 2D electron systems. *Europhys. Lett.* **106,** 47005 (2014).
29. Wang, T., Clark, K. P., Spencer, G. F., Mack, A. M. & Kirk, W. P. Magnetic field induced metal-insulator transition in two dimensions. *Phys. Rev. Lett.* **72,** 709–712 (1994).
30. *Perspectives in Quantum Hall Effects* (eds. Das Sarma, S. & Pinczuk, A.) (Wiley, New York, 1996).
31. Santos, M. B. *et al.* Observation of a reentrant insulating phase near the 1/3 fractional quantum Hall liquid in a two-dimensional hole system. *Phys. Rev. Lett.* **68,** 1188–1191 (1992).
32. Mani, R. G. *et al.* Zero-resistance states induced by electromagnetic wave excitation in GaAs/AlGaAs heterostructures. *Nature* **420,** 646–650 (2002).
33. Zudov, M. A., Du, R. R., Pfeiffer, L. N. & West, K. W. Evidence for a new dissipationless effect in 2D electronic transport. *Phys. Rev. Lett.* **90,** 046807 (2003).
34. Mani, R. G. *et al.* Demonstration of a 1/4 cycle phase shift in the radiation-induced oscillatory-magnetoresistance in GaAs/AlGaAs devices. *Phys. Rev. Lett.* **92,** 146801 (2004).
35. Mani, R. G. *et al.* Radiation-induced oscillatory magnetoresistance as a sensitive probe of the zero-field spin splitting in high-mobility GaAs/AlGaAs devices. *Phys. Rev. B* **69,** 193304 (2004).
36. Mani, R. G. Zero-resistance states induced by electromagnetic-wave excitation in GaAs/AlGaAs heterostructures. *Physica E (Amsterdam)* **22,** 1–6 (2004).
37. Kovalev, A. E., Zvyagin, S. A., Bowers, C. R., Reno, J. L. & Simmons, J. A. Observation of a node in the quantum oscillations induced by microwave radiation. *Sol. St. Comm.* **130,** 379–381 (2004).
38. Mani, R. G. Radiation-induced zero-resistance states with resolved Landau levels. *Appl. Phys. Lett.* **85,** 4962–4964 (2004).
39. Mani, R. G. Radiation-induced oscillatory magnetoresistance in a tilted magnetic field in GaAs/AlGaAs devices. *Phys. Rev. B* **72,** 075327 (2005).
40. Simovic, B., Ellenberger, C., Ensslin, K. & Wegscheider, W. Density dependence of microwave induced magnetoresistance oscillations in a two-dimensional electron gas. *Phys. Rev. B* **71,** 233303 (2005).
41. Smet, J. H. *et al.* Circular-polarization-dependent study of the microwave photoconductivity in a two-dimensional electron system. *Phys. Rev. Lett.* **95,** 116804 (2005).
42. Mani, R. G. Radiation-induced decay of Shubnikov-de Haas oscillations in the regime of the radiation-induced zero-resistance states. *Appl. Phys. Lett.* **91,** 132103 (2007).
43. Wirthmann, A. *et al.* Far-infrared-induced magnetoresistance oscillations in GaAs/AlGaAs-based two-dimensional electron systems. *Phys. Rev. B* **76,** 195315 (2007).
44. Wiedmann, S. *et al.* Interference oscillations of microwave photoresistance in double quantum wells. *Phys. Rev. B* **78,** 121301(R) (2008).
45. Mani, R. G., Johnson, W. B., Umansky, V., Narayanamurti, V. & Ploog, K. Phase study of oscillatory resistances in microwave irradiated and dark GaAs/AlGaAs devices: Indications of an unfamiliar class of integral quantum Hall effect. *Phys. Rev. B* **79,** 205320 (2009).
46. Wiedmann, S. *et al.* Magnetoresistance oscillations in multilayer systems: Triple quantum wells. *Phys. Rev. B* **80,** 245306 (2009).
47. Konstantinov, D. & Kono, K. Photon-induced vanishing of magnetoconductance in 2D electrons on liquid helium. *Phys. Rev. Lett.* **105,** 226801 (2010).
48. Mani, R. G., Gerl, C., Schmult, S., Wegscheider, W. & Umansky, V. Nonlinear growth with the microwave intensity in the radiation-induced magnetoresistance oscillations. *Phys. Rev. B* **81,** 125320 (2010).

49. Ramanayaka, A. N., Mani, R. G. & Wegscheider, W. Microwave induced electron heating in the regime of the radiation-induced magnetoresistance oscillations. *Phys. Rev. B* **83,** 165303 (2011).
50. Mani, R. G., Ramanayaka, A. N. & Wegscheider, W. Observation of linear-polarization-sensitivity in the microwave-radiation-induced magnetoresistance oscillations. *Phys. Rev. B* **84,** 085308 (2011).
51. Ramanayaka, A. N., Mani, R. G., Inarrea, J. & Wegscheider, W. Effect of rotation of the polarization of linearly polarized microwaves on the radiation-induced magnetoresistance oscillations. *Phys. Rev. B* **85,** 205315 (2012).
52. Mani, R. G., Hankinson, J., Berger, C. & de Heer, W. A. Observation of resistively detected hole spin resonance and zero-field pseudo-spin splitting in graphene. *Nature Commun.* **3,** 996, 10.1038/ncomms1986 (2012).
53. Mani, R. G. *et al.* Terahertz photovoltaic detection of cyclotron resonance in the regime of the radiation-induced magnetoresistance oscillations. *Phys. Rev. B* **87,** 245308 (2013).
54. Ye, T., Liu, H.-C., Wegscheider, W. & Mani, R. G. Combined study of microwave-power/linear polarization dependence of the microwave-radiation-induced magnetoresistance oscillations in GaAs/AlGaAs devices. *Phys. Rev. B* **89,** 155307 (2014).
55. Ye, T., Liu, H.-C., Wang, Z., Wegscheider, W. & Mani, R. G. Comparative study of microwave radiation-induced magnetoresistive oscillations induced by circularly- and linearly- polarized photoexcitation. *Sci. Rep.* **5,** 14880; 10.1038/srep14880 (2015).
56. Durst, A. C., Sachdev, S., Read, N. & Girvin, S. M. Radiation-induced magnetoresistance oscillations in a 2D electron gas, *Phys. Rev. Lett.* **91,** 086803 (2003).
57. Andreev, A. V., Aleiner, I. L. & Millis, A. J. Dynamical symmetry breaking as the origin of the zero-dc-resistance state in an ac-driven system. *Phys. Rev. Lett.* **91,** 056803 (2003).
58. Ryzhii, V. & Suris, R. Nonlinear effects in microwave photoconductivity of two-dimensional electron systems. *J. Phys.: Cond. Matt.* **15,** 6855–6869 (2003).
59. Koulakov, A. A. & Raikh, M. E. Classical model for the negative dc conductivity of ac-driven two-dimensional electrons near the cyclotron resonance. *Phys. Rev. B* **68,** 115324 (2003).
60. Lei, X. L. & Liu, S. Y. Radiation-induced magnetoresistance oscillation in a two-dimensional electron gas in Faraday geometry. *Phys. Rev. Lett.* **91,** 226805 (2003).
61. Torres, M. & Kunold, A. Kubo formula for Floquet states and photoconductivity oscillations in a two-dimensional electron gas. *Phys. Rev.* **B71,** 115313 (2005).
62. Inarrea, J. & Platero, G. Temperature effects on microwave-induced resistivity oscillations and zero-resistance states in two-dimensional electron systems. *Phys. Rev. B* **72,** 193414 (2005).
63. Lei, X. L. & Liu, S. Y. Radiation-induced magnetotransport in high mobility two-dimensional systems: Role of electron heating. *Phys. Rev. B* **72,** 075345 (2005).
64. Dmitriev, I. A., Vavilov, M. G., Aleiner, I. L., Mirlin, A. D. & Polyakov, D. G. Theory of microwave-induced oscillations in the magnetoconductivity of a two-dimensional electron gas. *Phys. Rev. B* **71,** 115316 (2005).
65. Inarrea, J. & Platero, G. Theoretical approach to microwave radiation-induced zero-resistance states in 2D electron systems. *Phys. Rev. Lett.* **94,** 016806 (2005).
66. Chepelianskii, A. D. & Shepelyansky, D. L. Microwave stabilization of edge transport and zero-resistance states. *Phys. Rev. B* **80,** 241308(R) (2009).
67. Dmitriev, I. A., Khodas, M., Mirlin, A. D., Polyakov, D. G. & Vavilov, M. G. Mechanisms of the microwave photoconductivity in two-dimensional electron systems with mixed disorder. *Phys. Rev. B* **80,** 165327 (2009).
68. Inarrea J., Mani, R. G. & Wegscheider, W. Sublinear radiation power dependence of photoexcited resistance oscillations in two-dimensional electron systems. *Phys. Rev. B* **82,** 205321 (2010).
69. Mikhailov, S. A. Theory of microwave-induced zero-resistance states in two-dimensional electron systems. *Phys. Rev. B* **83,** 155303 (2011).
70. Inarrea, J. Influence of linearly polarized radiation on magnetoresistance in irradiated two-dimensional electron systems. *Appl. Phys. Lett.* **100,** 242103 (2012).
71. Lei X. L. & Liu, S. Y. Linear polarization dependence of microwave-induced magnetoresistance oscillations in high mobility two-dimensional systems. *Phys. Rev. B* **86,** 205303 (2012).
72. Zhirov, O. V. Chepelianskii, A. D. & Shepelyansky, D. L. Towards a synchronization theory of microwave-induced zero-resistance states. *Phys. Rev. B* **88,** 035410 (2013).
73. Dai, Y., Du, R. R., Pfeiffer, L. N. & West K. W. Observation of a cyclotron harmonic spike in microwave-induced resistances in ultraclean GaAs/AlGaAs quantum wells. *Phys. Rev. Lett.* **105,** 246802 (2010).
74. Hatke, A. T., Zudov, M. A., Pfieffer, L. N. & West K. W. Giant microwave photoresistivity in high mobility quantum Hall systems. *Phys. Rev. B* **83** 121301 (2011).
75. Inarrea, J. Quenching of the giant off-resonance magnetoresistance spike mediated by an in-plane magnetic field in irradiated 2D-electron systems. *Phys. Lett. A* **377,** 2642–2646 (2013).
76. Warmenbol, P. Magnetophonon resonance condition in quasi one- and two-dimensional systems. In Spectroscopy of Semiconductor Heterostructures. *Proc. NATO Adv. Res. Workshop on Spectroscopy of Semiconductor Microstructures* (eds. Fasol, G., Fasolino, A. & Luigi P.) 11.98–11.133 (Springer Science + Business Media, New York, USA, 1989).
77. Asmar, N. G. *et al.* Temperature of quasi-two-dimensional electron gases under steady-state drive. *Appl. Phys. Lett.* **68,** 829 (1996).
78. Xu, W. & Zhang, C. Nonlinear transport in steady-state terahertz-driven two-dimensional electron gases. *Phys. Rev. B* **55,** 5259 (1997).
79. Yu, L. Y., Cao., J. C. & Zhang, C. Optical absorption coefficients in two-dimensiona semiconductors under strong magnetic field. *J. Appl. Phys.* **99,** 123706 (2006).
80. Dzurak, A. S. *et al.* Two-dimensional electron-gas heating and phonon emission by hot ballistic electrons. *Phys. Rev. B* **45,** 6309 (1992).

Acknowledgements

Research support has been provided by the ARO under W911NF-14-2-0076 and W911NF-15-1-0433. Magneto-transport studies in Georgia State University have been supported by the U.S. Department of Energy, Office of Basic Energy Sciences, Material Sciences and Engineering Division under DE-SC0001762.

Author Contributions

Measurements by Z.W. R.L.S. contributed to the discussion. Experimental development, data modeling, and manuscript by Z.W. and R.G.M. High quality GaAs/AlGaAs wafers due to C.R. and W.W.

Additional Information

Competing financial interests: The authors declare no competing financial interests.

How to cite this article: Wang, Z. *et al.* Tunable electron heating induced giant magnetoresistance in the high mobility GaAs/AlGaAs 2D electron system. *Sci. Rep.* **6**, 38516; doi: 10.1038/srep38516 (2016).